

Max-Margin Adversarial (MMA) Training: Direct Input Space Margin Maximization through Adversarial Training

Gavin Weiguang Ding, Yash Sharma, Kry Yik Chau Lui, and Ruitong Huang

Borealis AI

Abstract

Adversarial robustness is determined by the data points’ margins, the distances in the input space from the data points to the decision boundary of the classifier. We study the connection between directly maximizing these margins and adversarial training. In particular, we show that these two different objectives have aligned gradient. Furthermore, we show that directly maximizing margins is an improvement on adversarial training, in the sense that it can be interpreted as adversarial training with automatically selected “correct” perturbation magnitudes that are different for each individual data point. Motivated by our theoretical analysis, we propose the Max-Margin Adversarial (MMA) training to maximize the average margin. We demonstrate the efficiency of the MMA training framework on the MNIST and CIFAR10 datasets. On both, our MMA trained models obtain state-of-the-art robustness under various ℓ_∞ and ℓ_2 attacks. In particular, under the ℓ_∞ constraint with $\epsilon = 8/255$ on the CIFAR10 dataset, our MMA trained model achieved 9% higher robust accuracy than the best prior work reported in [Madry et al. \(2017\)](#).

1 Introduction

Despite their impressive performance on various learning tasks, neural networks have been shown to be vulnerable to adversarial perturbations ([Szegedy et al., 2013](#); [Biggio et al., 2013](#)). An artificially constructed perturbation, that is imperceptible to human, can cause a significant drop in the prediction accuracy of an otherwise accurate network. The accuracy on the perturbed data depends on the magnitude of the perturbations (e.g. in ℓ_∞ or ℓ_2 norms), which suggests the natural connection between adversarial robustness and the margins of the data points, i.e. the smallest distance from the sample points to the decision boundary induced by the network.

Not surprisingly, numerous algorithms in defending adversarial attacks have already been proposed in the literature which, arguably, can be interpreted as different ways in increasing the margins. One class uses regularization to constrain the model’s Lipschitz constant ([Cisse et al., 2017](#); [Ross and Doshi-Velez, 2017](#); [Hein and Andriushchenko, 2017](#); [Tsuzuku et al., 2018](#)), thus a sample with small loss would have a large margin since the loss cannot increase too fast. If the Lipschitz constant is regularized on the data points, it is usually too local and not accurate in a neighborhood; if it is controlled globally, the constraint on the model is often too strong that it harms accuracy. So far, such methods have not achieved strong robustness. There are also efforts using first-order approximation to estimate and maximize input space margin ([Elsayed et al., 2018](#); [Sokolic et al.,](#)

2017; Matyasko and Chau, 2017). Similar to local Lipschitz regularization, the reliance on local information might not provide accurate margin estimation and efficient maximization. Indeed, many defense methods have been broken after their proposal (Carlini and Wagner, 2016, 2017a; Athalye et al., 2018). Adversarial training (Huang et al., 2015; Madry et al., 2017) is one of the few which has stood the test of time, and in fact, represents the current SOTA results. However, as illustrated in Section 1.2, the update in adversarial training does not necessarily increase the margins, which in turn diminishes the effectiveness of adversarial training.

In this paper, we propose to directly maximize the margin on each training sample, called Max-Margin Adversarial (MMA) training, to achieve the greatest possible robustness on each individual example. Though seemingly intuitive, this formulation introduces technical difficulties in optimizing the objective. To see that, note that the new formulation (see Eq. (1) later in the paper) is a maxmin nested optimization problem with a constraint depending on the network parameter for the inner minimization.¹ Our theoretical analysis shows that under a smoothness assumption, our method, MMA training, uses the margin’s gradient, which is parallel to that of adversarial training when the perturbation budget of adversarial training is set to be the true margin. For the non-smooth losses, we show that the gradient from adversarial training is still positively related to that of our objective. Such a property makes gradient descent possible for the MMA objective, despite the model parameters are involved in the constraints.

We further take a deeper look at the connection between MMA training and adversarial training. Our analysis shows that MMA training is indeed an improvement over adversarial training, in the sense that

- Adversarial training with fixed perturbation length is maximizing a lower bound or upper bound of the margin, depending on if the margin of the data point is larger or smaller than ϵ ;
- MMA training is essentially doing adversarial training with automatically selected “correct” margin for each individual example.

We test our algorithms on MNIST and CIFAR10 under ℓ_∞ and ℓ_2 perturbations, demonstrating that our method outperforms previous adversarial training. Among all the cases, the most significant improvement is that our MMA trained model achieved 54.0 % whitebox robust accuracy under ℓ_∞ attack with $\epsilon = 8/255$ on the CIFAR10 dataset, which is about 9% higher than best prior work (45.2%), reported in Madry et al. (2017).

1.1 Notations

We focus on the K -class classification problem in this paper, and assume that the output of the model is a score function $\mathbf{f}_\theta(x) = (f_1(x), \dots, f_K(x))$ which assigns score $f_i(x)$ to the i th class. The predicted label of x is then decided by $\arg \max_i f_i(x)$. We use the “logit margin loss”² $L_\theta(x) = \max_{j \neq y} f_j(x) - f_y(x)$. Note that when $L_\theta(x) < 0$, the classification is correct, and when $L_\theta(x) > 0$, the classification is wrong. Given a model \mathbf{f}_θ and a data pair $z = (x, y)$, one can compute the *minimal length perturbation*, δ^* by

$$\delta^* = \arg \min_{\delta} \|\delta\| \quad \text{s.t. } L_\theta(x + \delta, y) \geq 0, \quad (1)$$

as illustrated in Figure 1. Denote the *margin* of example z by $d_\theta(z) = \|\delta^*\|$, which is the (minimal) distance from the input x to the decision boundary $L_\theta(z) = 0$ in the input space. Note that Eq. (1)

¹In adversarial training, the constraint on the inner maximization does NOT have such problem.

²Since the scores $(f_1(x), \dots, f_K(x))$ output by \mathbf{f} are also called logits in neural network literature.

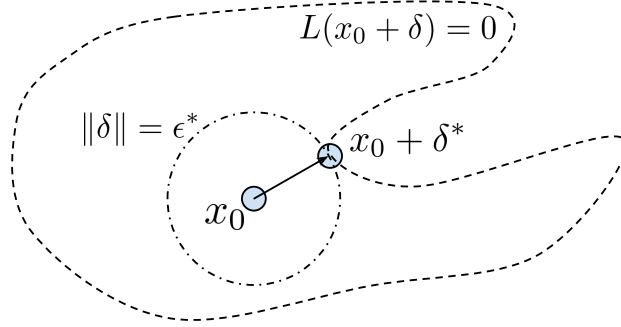


Figure 1: Illustration of decision boundary, minimal length perturbation, margin and etc.

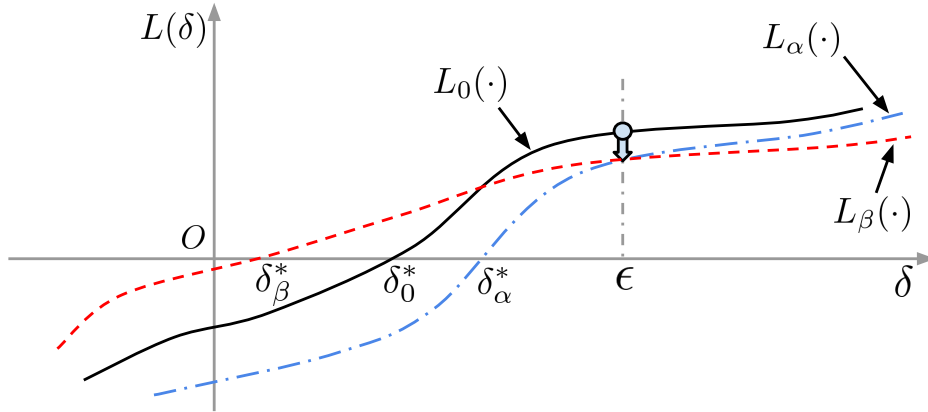


Figure 2: Fixed-norm adversarial training does not necessarily improve robustness.

is also compatible with misclassified samples, as for a sample z that is misclassified by \mathbf{f} , the optimal δ would be $\mathbf{0}$, hence $d_\theta(z) = 0$. Throughout this paper, we use the term “margin” to denote input space margin. For other notions of margin, we will use specific phrases, e.g. “output space margin” or “logit space margin.” All the proofs are postponed to Appendix A.

1.2 Adversarial Training Does NOT Necessarily Increase the Margin

We use an imaginary example in this section to illustrate that one update step of adversarial training does not necessarily increase the margin. Adversarial training (Huang et al., 2015) is based on a min-max formulation as

$$\min_{\theta} \max_{\|\delta\| \leq \epsilon} L_\theta(x + \delta, y) \quad (2)$$

where the “worst-case” loss is minimized under a fixed perturbation magnitude ϵ . Consider a one-dimensional example in Figure 2, where the input example x is a scalar. We perturb x in the positive direction with perturbation δ . We assume $L(\delta) = L_\theta(x + \delta, y)$ is monotonically increasing on δ , which means that the “larger” perturbation is always stronger.

Let $L_0(\cdot)$ denote the original function before an update step, and δ_0^* denote the corresponding margin (minimal length perturbation). Next, an update is made to the parameter of $L_0(\cdot)$, such that $L_0(\epsilon)$ is reduced. After this update, we imagine two different possibilities of the updated loss functions, $L_\alpha(\cdot)$ in blue dotted-dash line, and $L_\beta(\cdot)$ in red dash line. $L_\alpha(\epsilon)$ and $L_\beta(\epsilon)$ have the same decreased value at ϵ . However, we can see that $L_\alpha(\cdot)$ has an increased margin $\delta_\alpha^* > \delta_0^*$, but $L_\beta(\cdot)$

has a decreased margin $\delta_\beta^* < \delta_0^*$. The second case is undesirable since it is less robust as the margin decreases.

2 Margin Maximization

Here we discuss how to maximize margins on individual examples. Under a smooth assumption, we show how to calculate the gradient of the margin in Section 2.1. In Section 2.2 we show that margin maximization can still be achieved by loss minimization when the loss or the constraint norm is not smooth. We then discussed the relationship between margin maximization and adversarial training in Section 2.3.

2.1 Gradients of the Margins

Here we show how to calculate gradients of the margins, $\nabla d_\theta(z)$, on individual examples, as a preparation for presenting MMA training. Computing such gradients for a linear model is easy due to the existence of its closed-form solution, e.g. SVM. But it is not clear for general functions such as neural networks. Recall that $d_\theta(z) = \|\delta^*\| = \min_{L(\delta, \theta) \geq 0} \|\delta\|$, where we overload the loss notation with $L(\theta, \delta) = L_\theta(x + \delta, y)$ for simplicity, as we are considering a single example. It is easy to see that for a wrongly classified example z , δ^* is achieved at $\mathbf{0}$ and thus $\nabla_\theta d_\theta(z) = 0$. Therefore in this section, we focus on correctly classified data examples. Denote the Lagrangian as $\mathcal{L}(\delta, \lambda)$, where $\mathcal{L}(\delta, \lambda) = \|\delta\| + \lambda L(\delta, \theta)$. Also for a fixed θ , denote the optimizers of δ and λ by δ^* and λ^* . The following theorem provides an efficient way to compute $\nabla_\theta d_\theta(z)$.

Theorem 2.1. *Let $\epsilon(\delta) = \|\delta\|$. Given a fixed θ , assume that ϵ and $L(\delta, \theta)$ are C^2 functions at δ^* , and the matrix M is full rank, where*

$$M = \begin{pmatrix} \frac{\partial^2 \epsilon(\delta^*)}{\partial \delta^2} + \lambda^* \frac{\partial^2 L(\delta^*, \theta)}{\partial \delta^2} & \frac{\partial L(\delta^*, \theta)}{\partial \delta} \\ \frac{\partial L(\delta^*, \theta)}{\partial \delta}^\top & 0 \end{pmatrix}.$$

Then,

$$\nabla_\theta d_\theta(z) = C \frac{\partial L(\delta^*, \theta)}{\partial \theta},$$

$$\text{where } C = \frac{\left\langle \frac{\partial \epsilon(\delta^*)}{\partial \delta}, \frac{\partial L(\delta^*, \theta)}{\partial \delta} \right\rangle}{\left\| \frac{\partial L(\delta^*, \theta)}{\partial \delta} \right\|_2^2}.$$

2.2 Learning for Non-smooth Loss

Theorem 2.1 requires the loss function to be C^2 at δ^* . This might not be the case for piecewise C^2 functions, when δ^* is located right on the non-differentiable region, which could be the case for the popular ReLU networks. In this section we show that under weaker conditions, learning on θ to increase the margin of f_θ is still possible. Let $\ell_\epsilon(\theta) = \max_{\delta \in [-\epsilon, \epsilon]^d} L(\delta, \theta)$. Given the current parameter θ_0 , let $\delta^* = \arg \max_{\delta \in [-\epsilon, \epsilon]^d} L(\delta, \theta_0)$. In particular, we show that there always exists a direction d and a proper step size t such that $\ell_\epsilon(\theta_0 + t\vec{d}) < \ell_\epsilon(\theta_0)$, if θ_0 is not local minimum of $\ell_\epsilon(\theta)$. We then show that if ϵ is the margin of f_{θ_0} , then $\ell_\epsilon(\theta_0 + t\vec{d}) < \ell_\epsilon(\theta_0)$ implies that $f_{\theta_0 + t\vec{d}}$ has a larger margin than f_{θ_0} . Therefore, learning on θ to maximize the margin can be done by decreasing $\ell_{\epsilon_0}(\theta)$ where ϵ_0 is the margin of the current parameter θ_0 .

For simplicity, consider a K -layers fully-connected ReLU network, $f(\theta; x) = f_\theta(x)$ as a function of θ .

$$f(\theta; x) = V^\top D_K W_K D_{K-1} W_{K-1} \cdots D_1 W_K^\top x \quad (3)$$

where the D_k are diagonal matrices depend on ReLU's activation pattern over the layers, and W_k 's and V are the weights (i.e. θ). Note that $f(\theta; x)$ is a piecewise polynomial functions of θ with finitely many pieces. We further define the directional derivative of a function g , along the direction of \vec{d} , to be:

$$g'(\theta; \vec{d}) := \lim_{t \downarrow 0} \frac{g(\theta + t\vec{d}) - g(\theta)}{t}.$$

Note that for every direction \vec{d} , there exists $\alpha > 0$ such that $f(\theta; x)$ is a polynomial restricted to a line segment $[\theta, \theta + \alpha\vec{d}]$. Thus the above limit exists and the directional derivative is well defined.

We first show the existence of \vec{d} and t for $\ell_\epsilon(\theta_0 + t\vec{d})$ given any ϵ . Let $\ell_{\theta_0, \vec{d}, \epsilon}(t) := \sup_{\delta \in [-\epsilon, \epsilon]^d} L(\delta, \theta_0 + t\vec{d})$.

Proposition 2.1. *For $\epsilon > 0$, $t \in [0, 1]$, and $\theta_0 \in \Theta$, there exists a direction $\vec{d} \in \Theta$, such that the derivative of $\ell_{\vec{d}, \epsilon, \theta_0}(t)$ exists and is negative. Moreover, it is given by*

$$\ell'_{\vec{d}, \epsilon, \theta_0}(t) = L'(\delta^*, \theta_0; \vec{d}).$$

Therefore, for any $\epsilon > 0$, if θ_0 is not a local minimum, then there exists a direction d , such that for $\theta_1 = \theta_0 + t\vec{d}$ for a proper t ,

$$\sup_{\delta \in [-\epsilon, \epsilon]^d} L(\delta, \theta_0 + t\vec{d}) < \sup_{\delta \in [-\epsilon, \epsilon]^d} L(\delta, \theta_0). \quad (4)$$

Our next proposition provides an alternative way to increase the margin of f_θ .

Proposition 2.2. *Assume f_{θ_0} has a margin ϵ_0 , and θ_1 such that $\ell_{\theta_0, \vec{d}, \epsilon_0}(t) \leq \ell_{\theta_1, \vec{d}, \epsilon_0}(0)$, then f_{θ_1} has a larger margin than ϵ_0 .*

Therefore, the update $\theta_0 \rightarrow \theta_1 = \theta_0 + t\vec{d}$ increases the margin of f_θ .

2.3 Relation to Standard Adversarial Training

As suggested by Theorem 2.1, MMA training is closely related to adversarial training. In this section, we reveal a deeper connection between them.

Given a sample $z = (x, y)$ and a fixed length ϵ , recall that adversarial training learns a model \mathbf{f} by minimizing the adversarial loss,

$$\min_{\theta} J_\theta(\epsilon) = \min_{\theta} \max_{\|\delta\| \leq \epsilon} L_\theta(x + \delta, y)$$

For simplicity, we denote $L_\theta(x + \delta, y)$ by $L_\theta(\delta)$ in this section. Further let $\epsilon^*(\ell) = \min_{\delta: L_\theta(\delta) = \ell} \|\delta\|$ be the minimal magnitude to reach the level set of $L_\theta(\delta) = \ell$. For a given (x, y) and a fixed perturbation magnitude ϵ , assume that $\ell^* = \max_{\|\delta\| \leq \epsilon} L_\theta(\delta)$. Note that with a surrogate loss $\tilde{L}_\theta(\delta) = L_\theta(\delta) - \ell^*$ and by the claim in Section 2.2, adversarial training is equivalent to enlarging $\epsilon^*(\ell^*)$. Note that $\epsilon^*(\ell^*) < \epsilon^*(0)$ if $\ell^* < 0$, and $\epsilon^*(\ell^*) > \epsilon^*(0)$ if $\ell^* > 0$. Therefore, adversarial training can be interpreted as that:

Algorithm 1 Adaptive Norm PGD Attack.

Inputs: (x, y) is the data example. ϵ_{init} is the initial norm constraint used in the first PGD attack.

Outputs: δ^* , approximate shortest successful perturbation.

Parameters: ϵ_{max} is the maximum perturbation length. $\text{PGD}(x, y, \epsilon)$ represents PGD (Madry et al., 2017) perturbation δ with maximum perturbation length ϵ .

- 1: Adversarial example $\delta_1 = \text{PGD}(x, y, \epsilon_{init})$
 - 2: Unit perturbation $\delta_u = \frac{\delta_1}{\|\delta_1\|}$
 - 3: **if** prediction on $x + \delta_1$ is correct **then**
 - 4: $\epsilon' = \|\arg \min_{\eta} |L(x + \eta\delta_u, y)|\|, \eta \in [\epsilon_{init}, \epsilon_{max}]$
 - 5: **else**
 - 6: $\epsilon' = \|\arg \min_{\eta} |L(x + \eta\delta_u, y)|\|, \eta \in [0, \epsilon_{init}]$
 - 7: **end if**
 - 8: $\delta^* = \epsilon'\delta_u$
-

Adversarial training with fixed perturbation length is maximizing a lower bound or upper bound of the margin, depending on if the margin of the data point is larger or smaller than ϵ .

Moreover, our next two results show that MMA training is essentially doing adversarial training with the “correct” margin for each individual example.

Theorem 2.2. Let $\theta_{MMA} = \arg \max_{\theta} \min_{L_{\theta}(\delta) \geq \ell} \|\delta\|$, with the assumption that $\ell \geq L_{\theta}(0) \in \text{Range}(L_{\theta})$. Also let $\theta_{adv} = \arg \min_{\theta} \max_{\|\delta\| \leq \epsilon^*} L_{\theta}(\delta)$, and $\epsilon^* = \min_{L_{\theta_{MMA}}(\delta) \geq \ell} \|\delta\|$, then θ_{MMA} also minimizes the adversarial loss, i.e.

$$\max_{\|\delta\| \leq \epsilon^*} L_{\theta_{MMA}}(\delta) = \max_{\|\delta\| \leq \epsilon^*} L_{\theta_{adv}}(\delta).$$

Our next theorem shows that if ϵ is picked “tightly”, then the optimal \mathbf{f} that minimizes the adversarial loss also maximizes the margin given the corresponding threshold ℓ^* .

Theorem 2.3. Let $\theta_{adv} = \arg \min_{\theta} \max_{\|\delta\| \leq \epsilon} L_{\theta}(\delta)$, with $\epsilon \geq 0$. Also let $\ell^* = \max_{\|\delta\| \leq \epsilon} L_{\theta_{adv}}(\delta)$, and $\theta_{MMA} = \arg \max_{\theta} \min_{L_{\theta}(\delta) \geq \ell^*} \|\delta\|$. Further assume that

$$\min_{L_{\theta_{adv}}(\delta) \geq \ell^*} \|\delta\| = \epsilon, \quad (\text{No overshooting assumption})$$

then θ_{adv} also maximizes the margin distance, i.e.

$$\min_{L_{\theta_{adv}}(\delta) \geq \ell^*} \|\delta\| = \min_{L_{\theta_{MMA}}(\delta) \geq \ell^*} \|\delta\|.$$

Theorems 2.2 and 2.3 suggest that:

MMA training can also be interpreted as a way of improving adversarial training by finding the proper ϵ for each training sample, which is exactly the flavor of Algorithm 2.

Algorithm 2 Max-Margin Adversarial Training.

Inputs: The training set $\{(x_i, y_i)\}$.

Outputs: the trained neural network model $f_\theta(\cdot)$.

Parameters: ϵ contains perturbation lengths of training data. ϵ_{min} is the minimum perturbation length. ϵ_{max} is the maximum perturbation length. $\mathcal{A}(x, y, \epsilon_{init})$ represents the approximate minimal length perturbation returned by the algorithm \mathcal{A} on the data example (x, y) and at the initial norm ϵ_{init} .

- 1: Randomly initialize the parameter θ of model f , and initialize every element of ϵ as ϵ_{min}
 - 2: **repeat**
 - 3: Read minibatch $B = \{(x_1, y_1), \dots, (x_m, y_m)\}$
 - 4: Make predictions on B and into two: wrongly predicted B_0 and correctly predicted B_1
 - 5: **for** (x_i, y_i) in B_1 **do**
 - 6: Retrieve perturbation length ϵ_i from ϵ
 - 7: $\delta_i^* = \mathcal{A}(x_i, y_i, \epsilon_i)$
 - 8: Update the ϵ_i in ϵ as $\|\delta_i^*\|$, and put $(x_i + \delta_i^*, y_i)$ into B_1^{adv}
 - 9: **end for**
 - 10: Calculate the gradient of margin on B_1^{adv} and the gradient of classification loss on B_0
 - 11: Perform one step gradient step update on θ
 - 12: **until** meet training stopping criterion
-

3 Max-Margin Adversarial Training

This section is devoted to the presentation of MMA training. Motivated by the observation in Section 1.2, MMA training directly uses margins in its objective:

$$\min_{\theta} \left\{ \sum_{i \in \mathcal{S}_\theta^+} \max\{0, d_{\max} - d_\theta(z_i)\} + \sum_{j \in \mathcal{S}_\theta^-} \mathcal{J}_\theta(z_j) \right\}, \quad (5)$$

where $\mathcal{J}_\theta(\cdot)$ is a regular classification loss function, e.g. cross-entropy loss, which can be different from $L_\theta(\cdot)$. The margin $d_\theta(z_i)$ is inside the hinge loss with threshold d_{\max} , which means that the margin will be maximized when $d_\theta(z_i) < d_{\max}$. $\mathcal{S}_\theta^+ = \{i : L_\theta(z_i) < 0\}$ is the set of all correctly classified examples, and $\mathcal{S}_\theta^- = \{i : L_\theta(z_i) \geq 0\}$ is the set of wrongly classified examples. Intuitively, MMA training tries to minimize classification loss on wrongly classified examples in \mathcal{S}_θ^- , until they are correctly classified. For already correctly classified examples, MMA training tries to maximize the margin $d_\theta(z_i)$. Note that we do not maximize margins on wrongly classified examples, since the gradient of their margins are $\mathbf{0}$, as we discussed in Section 2.1.

To minimize Eq. (5), first note that $\nabla_\theta \mathcal{J}_\theta(z_j)$ can be easily computed by standard back-propagation. For the term of $d_\theta(z_i)$, as discussed in Theorem 2.1 and Section 2.2, one can instead update θ with the gradient of the adversarial loss at the minimal length perturbation δ^* .

In practice, we find that the gradient of the ‘‘logit margin loss’’ $\text{LM}(o) = \max_{i \neq y} o_i - o_y$ is not stable. Indeed, the gradient of LM is a piecewise constant function which suffers large fluctuations on the boundary of the pieces. It also does not fully utilize information provide by all the logits.

We instead consider a ‘‘soft logit margin loss’’ (SLM), $\text{SLM}(o) = \log \sum_{i \neq y} \exp(o_i) - o_y$, which replaces the max function by a ‘‘LogSumExp’’ function. The next proposition shows the close connection between SLM and LM, also between SLM and cross-entropy (CE).

Proposition 3.1. Let $SLM(o) = \log \sum_{i \neq y} \exp(o_i) - o_y$. Then for any o ,

$$SLM(o) - \log(K) \leq LM(o) \leq SLM(o),$$

where K is the dimension of o . Moreover, $\nabla_o CE(o) = r \nabla_o SLM(o)$, where $r = \frac{\sum_{i \neq y} \exp(o_i)}{\sum_i \exp(o_i)}$

Proposition 3.1 shows two ideal properties of SLM: 1) SLM upper bounds LM, and $SLM - \log(K)$ lower bounds LM; 2) SLM and CE always have same gradient direction. Due to property 1), the margin defined with SLM will be a lower bound of the margin defined with LM. Therefore, SLM can be used as a surrogate loss to perform margin maximization, while maintaining the theoretical guarantees. This involves finding δ^* with $\delta^* = \arg \min_{SLM_\theta(x+\delta, y) \geq 0} \|\delta\|$, and minimize the loss $SLM_\theta(\delta^*)$ w.r.t θ . Due to 2), once we find the δ^* , we can use CE instead of SLM to minimize the loss $CE_\theta(\delta^*)$ w.r.t θ , which provides the nice gradient scaling property of CE in training. In practice, we SLM to find δ^* , and then perform gradient descent on model parameters using $CE_\theta(\delta^*)$. Therefore, the MMA training objective can be written as:

$$\min_{\theta} \left\{ \sum_{i \in \mathcal{S}_\theta^+} CE_\theta(x_i + \delta^*, y_i) + \sum_{j \in \mathcal{S}_\theta^-} CE_\theta(z_j) \right\}, \quad (6)$$

where $\delta^* = \arg \min_{SLM_\theta(x+\delta, y) \geq 0} \|\delta\|$ is found with the SLM loss, and $\mathcal{H}_\theta = \{i : d_\theta(z_i) < d_{\max}\}$ is the set of examples that has margin smaller than the hinge threshold.

To implement MMA, we still need to find the δ^* , which is intractable in general settings³. We propose an adaptation of the projected gradient descent (PGD) attack to give an approximate solution of δ^* , the Adaptive Norm Projective Gradient Descent Attack (AN-PGD). In AN-PGD, we apply PGD (Madry et al., 2017) on a initial perturbation magnitude ϵ_{init} to find a norm-constrained perturbation δ_1 , then we search along the direction of δ_1 to find a scaled perturbation that gives $L = 0$, we then use this scaled perturbation to approximate ϵ^* . Algorithm 1 describes the details.⁴

To summarize, MMA training can be easily implemented as described in Algorithm 2. Note that AN-PGD here only serves as an algorithm to give an approximate solution of δ^* , and it can be decoupled from the rest parts of MMA training. Other attacks that can serve a similar purpose can also fit into our MMA training framework, e.g. the Decoupled Direction and Norm (DDN) attack (Rony et al., 2018).

4 Experiments

We test MMA training on the MNIST and CIFAR10 datasets under ℓ_∞ and ℓ_2 perturbations.

Models and training: We train LeNet5 models for the MNIST experiments and use wide residual networks (Zagoruyko and Komodakis, 2016) with depth 28 and widen factor 4 for all the CIFAR10 experiments. Details of network structures, attack and training hyperparameters can be found in Appendix B. For all the experiments, we monitor the average margin from AN-PGD on the validation set⁵ and choose the model with largest average margin from the sequence of checkpoints

³Exceptions exist, for example linear SVM.

⁴The zero-crossing binary search is denoted as $\arg \min_{\eta} |L(\eta)|$ for brevity.

⁵The validation set contains first 5000 images of training set. It is only used to monitor training progress and not used in training.

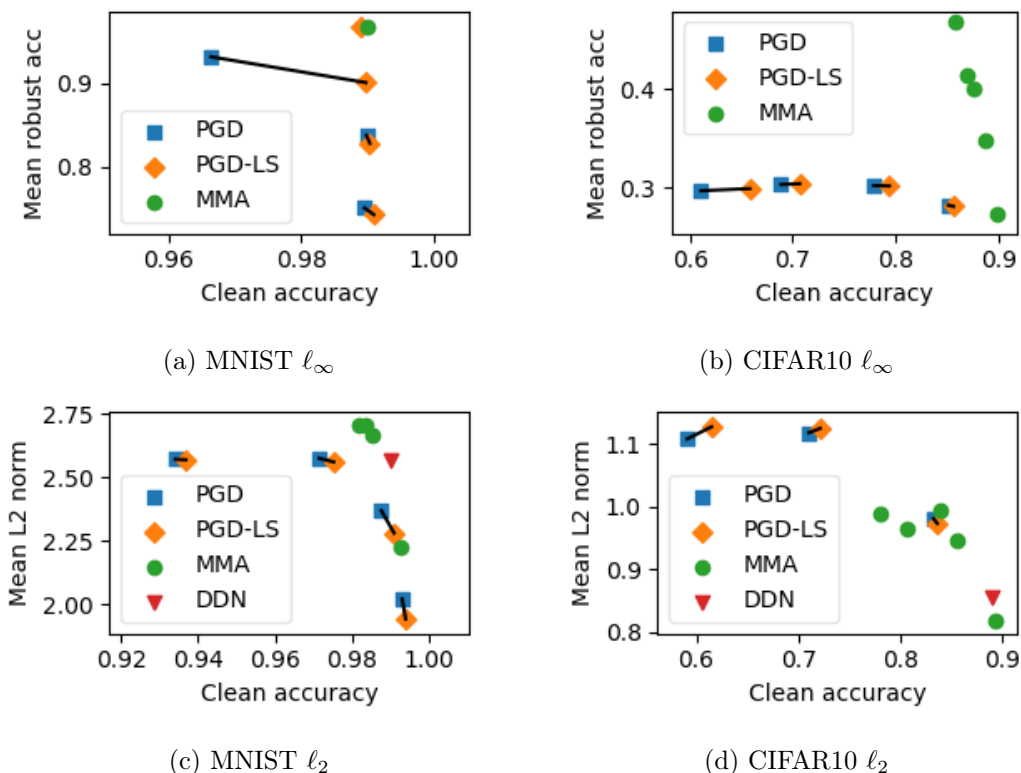


Figure 3: Accuracy vs robustness plots for models trained under different settings. In the legends, MMA represents MMA trained models; PGD represents PGD trained models with fixed perturbation magnitudes from the beginning; PGD-LS represents PGD trained models with gradually linearly increased perturbation magnitudes; for ℓ_2 cases, DDN represent DDN trained models. Black lines connects PGD and PGD-LS models with the same hyperparameters.

during training. Here all the models are trained and tested under the same type of norm constraints.⁶

Baselines from existing literature: Under all dataset and norm settings, we use PGD training (Madry et al., 2017) as a baseline.⁷ For ℓ_2 robustness, we also compare to models adversarially trained on the “Decoupled Direction and Norm” (DDN) attack (Rony et al., 2018), which is concurrent to our work. DDN attack aims to achieve successful perturbation with minimal ℓ_2 norm, which makes DDN training very similar to our MMA training. In fact, DDN attack could be a drop-in replacement for the AN-PGD attack for MMA training. We performed evaluations on the downloaded⁸ DDN trained models. For both MNIST and CIFAR10, the downloaded DDN models are larger models than ours. We further compare MMA with DDN training in Appendix C.

A new baseline, PGD training with gradually increasing global perturbation magnitude: As shown in Section 2.3, PGD training can be seen as maximizing the lower bound of the margin if the perturbation magnitude is smaller than the margin. Therefore, PGD with gradually increasing perturbation magnitude from small values can be interpreted as maximizing the lower

⁶If train on ℓ_∞ , then test on ℓ_∞ ; if train on ℓ_2 , then test on ℓ_2 .

⁷We also provide results on standardly trained models in Table 3 and Table 4 for references in the appendix.

⁸github.com/jeromerony/fast_adversarial

bound of the margin and continues as long as the increased perturbation magnitude is below the actual margin. Such method could provide better performance than PGD with a fixed large magnitude, as it makes more sense than maximizing upper bounds of the margins if the fixed magnitude is larger than the margins. With such analysis, we propose linear scaling PGD (PGD-LS) training as a new baseline. For all the PGD-LS training experiments, the magnitude of the norm constraint grows from 0 to the fixed magnitude linearly in 50 epochs. PGD-LS training can also be seen as a “global magnitude scheduling” training method to compare with MMA training, which can be seen as magnitude scheduling on each individual examples.

Evaluation under ℓ_∞ perturbation: We use projected gradient descent (PGD) (Madry et al. (2017)) to evaluate the ℓ_∞ robustness of models. Regarding the loss function of PGD, we use both the cross-entropy (CE) loss and the Carlini and Wagner (CW) loss.⁹ We consider the mean robust accuracy under different perturbation magnitudes as our robustness measure in Figure 3a and 3b. Specifically, for MNIST, we perform CE-PGD and CW-PGD attacks from $\epsilon = 0.05$ to $\epsilon = 0.4$ at a 0.05 interval, we then use stronger one among the CE-PGD and CW-PGD perturbations, to achieve the robust accuracy at each ϵ . Robust accuracies across all these 8 magnitudes (from 0.05 to 0.4) are then averaged as the mean robust accuracy used as the vertical axis in Figure 3a. Similarly, for CIFAR10, the mean robust accuracy is the average robust accuracies on magnitudes from 2 to 32 at a interval of 2 (totally 16 magnitudes). The PGD attacks run 100 iterations on MNIST and 20 iterations on CIFAR10.

To thoroughly examine the whitebox robustness of models, we choose $\epsilon = 0.3$ and $\epsilon = 0.4$ as representative magnitudes for MNIST, and perform 50 random restarts of CE-PGD and 50 random restarts of CW-PGD. Similarly for CIFAR10, we choose $\epsilon = 8/255$ and $\epsilon = 16/255$, and perform 10 restarts of each. Representative results are shown in Table 1. Full results are delayed to Table 3 in the appendix.

Evaluation under ℓ_2 perturbation: We use DDN attack and the Carlini and Wagner (CW) attack to evaluate the robustness trained under ℓ_2 setting. Note here for ℓ_2 setting, we use the CW attack, where for ℓ_∞ we use PGD with the CW “loss”. The robustness of models are quantified by attack success rate (ASR) and mean ℓ_2 norm of successful attacks. Besides considering the ASR and mean norm from DDN and CW individually, we also combine DDN and CW attack to take strongest attack, by picking shortest successful attacks from the 2 attacks they generated on the same input example. In Figure 3c and 3d, we use mean ℓ_2 norm (of the combined DDN and CW attack) as the robust measure. Table 2 contains representative results with ASR and mean ℓ_2 norm from DDN, CW and combined attacks on various models. Full results are delayed to Table 4 in the appendix.

4.1 Results and Analysis

MNIST under ℓ_∞ perturbation: Here we only trained one instance of MMA model with hinge threshold $d_{\max} = 0.45$. For PGD and PGD-LS, we trained models with $\epsilon = 0.3, 0.35, 0.4, 0.45$. From Figure 3a and Table 1, we can see that the best two models under this settings are the

⁹The CW loss is almost equivalent to the logit margin (LM) loss. We use CW loss for the ease of comparing with literature. Here $CW(x) = \min\{\max_{j \neq y} f_j(x) - f_y(x), 0\}$. When the classification is correct, CW and LM loss have the same gradient.

¹⁰Model from Madry et al. (2017). The accuracies of “100-step PGD on the cross-entropy loss with 50 random restarts” is from github.com/MadryLab/mnist_challenge/

¹¹Model from Madry et al. (2017). The accuracy of “20-step PGD on the cross-entropy loss with 10 random restarts” is from github.com/MadryLab/cifar10_challenge/

Table 1: Accuracy and Robustness of models under ℓ_∞ training. In the model column, M- d_{\max} represents the MMA trained model with hinge threshold d_{\max} . PL- ϵ represents the PGD trained model with linear magnitude scaling. P- ϵ represents the PGD trained model with fixed ϵ magnitude. PGDm shows the performances reported in Madry et al. (2017). CE represents robust accuracies after 50 random starts of PGD attacks cross-entropy loss. CW represents robust accuracies after 50 random starts of PGD attacks with CW loss. BOTH represents the accuracy under combined CE and CW (100 random starts) PGD attacks.

MNIST MODEL	ACC	ACC AT $\epsilon = 0.3$			ACC AT $\epsilon = 0.4$		
		CE	CW	BOTH	CE	CW	BOTH
M-0.45	99.0	93.7	93.7	93.6	89.0	89.1	88.6
PL-0.45	98.9	94.3	94.4	94.2	90.2	90.3	89.9
PL-0.4	99.0	93.8	93.9	93.8	89.5	89.7	89.2
P-0.4	96.6	88.7	88.7	88.5	84.6	84.5	84.1
PGDm ¹⁰	98.8	89.6	89.7	–	–	–	–
CIFAR MODEL	ACC	ACC AT $\epsilon = 8/255$			ACC AT $\epsilon = 16/255$		
		CE	CW	BOTH	CE	CW	BOTH
M-32	85.8	55.2	54.9	54.0	41.5	38.9	37.8
M-20	87.0	53.3	53.6	52.3	35.9	33.5	32.4
PL-20	65.8	48.3	45.1	44.8	30.5	26.4	25.3
PL-12	79.4	51.8	50.2	49.2	23.5	23.1	21.3
PL-8	85.6	49.8	49.1	47.7	16.6	17.3	15.6
P-20	61.1	46.3	43.4	43.2	31.8	27.6	26.7
P-16	77.9	51.8	49.9	49.0	24.5	24.0	22.1
PGDm ¹¹	87.3	45.2	–	–	–	–	–

MMA and PGD-LS with $\epsilon = 0.45$. Both models are very robust under attacks with $\epsilon = 0.3, 0.4$, with PGD-LS-0.45 slightly better than MMA-0.45. On the other hand, PGD-0.45, PGD training with no scheduling with $\epsilon = 0.45$, did not converge during training, therefore does not appear in Figure 3a, Table 1 and 3. The ϵ linear scheduling also help improves PGD-LS-0.4 (with scheduling) over PGD-0.4 (no-scheduling) at $\epsilon = 0.4$. However, if the magnitude is small, when $\epsilon = 0.3, 0.35$, magnitude scheduling does not help.

The success of PGD-LS and MMA verifies our analysis in Section 1.2 and 2.3. Recall that PGD training with a magnitude larger than the actual margin is roughly equivalent to maximizing a upper bound of the margin. If this magnitude is too large, then the upper bound of the margin and the margin will be almost “irrelevant”, therefore PGD will not make progress on the actual margin value. Likely due to this, the PGD-0.45 model did not converge. However, when the global perturbation magnitude scheduling is proper, in the case of PGD-LS-0.45, PGD-LS training can achieve similar, even slightly better performance than MMA. This might be due to that adversarial robustness under the MNIST ℓ_∞ case is a “easy” task. As we show later, MMA usually outperforms PGD-LS in other cases.

CIFAR10 under ℓ_∞ perturbation: We train MMA models with hinge threshold 8/255, 12/255, 16/255, 20/255, 32/255. For PGD and PGD-LS, we train with perturbation magnitude 8/255, 12/255, 16/255, 20/255. From Figure 3b and Table 1, we can observe the tradeoff between accuracy and robustness when the hinge threshold changes: the higher d_{\max} is, the more robust the trained model is, and the less accurate it is. When d_{\max} changes from 8/255 to 32/255, the mean robust accuracy increased significantly from below 30% to higher than 45%, while the clean accuracy only dropped from 89.8% to 85.8%. On the other hand, increasing the perturbation magnitude in

Table 2: Accuracy and Robustness of models under ℓ_2 training. In the model column, M- d_{\max} , PL- ϵ , P- ϵ have the same meaning as those in Table 1. DNN represents our evaluation on models from Rony et al. (2018) ASR is attack success rate (lower the better). DDN represents the ASR/mean norm after DDN attack with 1000 iterations. CW represents the ASR/mean norm after CW attack 9×10000 iterations. BOTH represents the ASR/mean norm after picking the stronger attack among DDN and CW attack.

MNIST MODEL	Acc	ASR			MEAN ℓ_2		
		DDN	CW	BOTH	DDN	CW	BOTH
M-8	98.2	100.0	99.8	100.0	2.72	2.81	2.71
M-6	98.3	100.0	99.0	100.0	2.72	2.85	2.71
M-4	98.5	100.0	98.6	100.0	2.68	2.80	2.67
M-2	99.3	100.0	100.0	100.0	2.24	2.26	2.23
PL-4	93.7	100.0	100.0	100.0	2.82	2.67	2.57
PL-1	99.1	100.0	100.0	100.0	2.30	2.32	2.28
P-4	93.4	100.0	100.0	100.0	2.84	2.68	2.57
P-1	99.3	100.0	100.0	100.0	2.04	2.04	2.02
DDN	99.0	100.0	100.0	100.0	2.61	2.63	2.57
CIFAR MODEL	Acc	ASR			MEAN ℓ_2		
		DDN	CW	BOTH	DDN	CW	BOTH
M-7	78.0	96.2	100.0	100.0	1.67	1.14	0.99
M-5	80.6	97.0	100.0	100.0	1.77	1.13	0.97
M-3	83.8	98.4	100.0	100.0	1.13	1.11	1.00
M-1	89.4	100.0	100.0	100.0	0.82	0.84	0.82
PL-3	61.5	100.0	100.0	100.0	1.30	1.16	1.13
PL-2	72.1	100.0	100.0	100.0	1.22	1.17	1.13
PL-1	83.6	100.0	100.0	100.0	1.01	1.02	0.97
P-3	59.1	100.0	100.0	100.0	1.29	1.14	1.11
P-2	71.1	100.0	100.0	100.0	1.21	1.17	1.12
P-1	83.2	100.0	100.0	100.0	1.01	1.03	0.98
DDN	89.1	100.0	100.0	100.0	0.86	0.89	0.86

PGD and PGD-LS decreases clean accuracy significantly but only gain little improvement in the overall robustness. In Table 1, although PGD-LS-20 has certain degree of robustness, 44.8 % at $\epsilon = 8/255$ and 25.3% at $\epsilon = 16/255$, the clean accuracy is reduced to 65.8%. In contrast, MMA-20 is better than all the PGD/PGD-LS models on both accuracy and robustness at $\epsilon = 8/255, 16/255$. Notably, our MMA trained model MMA-32 achieved 54.0% robust accuracy against $\epsilon = 8/255$ and 37.8% against $\epsilon = 16/255$, while still maintaining the 85.8 clean accuracy. To the best of our knowledge, this is currently the best whitebox robustness results on CIFAR10 with $\ell_\infty \epsilon = 8/255$ and $\epsilon = 16/255$. Regarding the effect of magnitude scaling, from Figure 3b we can see that PGD-LS does help the model to achieve better clean accuracy, but with almost no effect on increasing the model’s robustness.

MNIST under ℓ_2 perturbation: Here we train MMA models with hinge threshold 2, 4, 6, 8, and PGD/PGD-LS models with perturbation magnitude 1, 2, 3, 4. We also compare to the downloaded DDN trained model. From Figure 3c and Table 2, we can see that the PGD-LS models tends to have better accuracy and lower robustness than PGD models, but the difference is not significant. MMA models and DDN model in general achieves better tradeoff. Under a similar accuracy to PGD/PGD-LS models, MMA/DDN models have higher robustness. Also under a similar robustness to PGD/PGD-LS models, MMA/DDN models have higher accuracy. For example, PGD-LS-4 and MMA-4 achieved similar mean ℓ_2 norm (2.57 vs 2.67), but PGD-LS-4 sacrifices significantly in

accuracy compared to MMA-4 (93.7% vs 98.5%). The DDN trained model has similar performance to MMA models, with slightly different tradeoff on robustness vs accuracy, i.e. DDN has better accuracy over MMA-8/MMA-6/MMA-4 (99.0% vs 98.2%/98.3%/98.5%) and slightly worse mean ℓ_2 norm than MMA-8/MMA-6 (2.57 vs 2.71/2.71/2.67). This is not surprising since DDN adversarial training is a very similar training algorithm to MMA training as discussed previously.

We also noticed that although from MMA-2 to MMA-4 the mean ℓ_2 norm increase significantly from 2.23 to 2.67, further increased hinge threshold does not significantly change either the clean accuracy or the mean ℓ_2 norm. This might be due to the intrinsic difficulty of achieving both accuracy and robustness at the same time (Tsipras et al., 2019).

CIFAR10 under ℓ_2 perturbation: Under this case, we train MMA models with hinge threshold 1, 2, 3, 5, 7 and PGD/PGD-LS models with perturbation magnitude 1, 2, 3. Similar to MNIST ℓ_2 , PGD/PGD-LS models exhibits strong robustness-accuracy tradeoffs, the DDN model trained roughly has similar level of robustness-accuracy tradeoff to MMA trained models, as it can be seen from Table 2. Here the MMA trained models show typical robustness-accuracy tradeoff when the hinge threshold is smaller than 3. When the threshold is at 5, 7, the accuracy drops but the robustness does not increase. Due to the different robustness-accuracy tradeoff properties, it is only easy to compare MMA-3 with PGD-LS-1/PGD-1, where MMA-3 has both better accuracy (83.8% vs 83.6%/83.2%) and robustness (1.00 vs 0.97/0.98).

4.2 Summary of Results

Effect of global magnitude scheduling on PGD training: From Figure 3, we can see that PGD-LS helps under the majority of the cases. Specifically, under all PGD/PGD-LS pairs, PGD-LS improves models’ clean accuracies, sometimes at cost of reduced robustness. The most significant improvement with PGD-LS are the PGD-LS-0.45 and PGD-LS-0.4 cases under MNIST ℓ_∞ , where PGD-0.45 training did not converge and PGD-0.4 model has significantly worse clean accuracy than PGD-LS-0.4.

MMA training vs PGD training: Under ℓ_∞ scenarios, MMA performs significantly better than regular PGD training. The proposed PGD-LS baseline performs slightly better than MMA in the MNIST ℓ_∞ case. However, since PGD-LS is motivated by our “lower bound” analysis in Section 1.2 and 2.3, this behavior is well predicted by our theory. On the other hand, MMA performs significantly better than PGD-LS under CIFAR10 ℓ_∞ , which substantially demonstrate the potential of MMA. Under ℓ_2 scenarios, MMA usually achieves a better robustness-accuracy tradeoff, which is reflected as appearing at the top-right directions to nearby PGD/PGD-LS trained models, in Figure 3c and 3d.

5 Related Works

We discuss a few related works in details here.

First-order Large Margin: Previous works (Elsayed et al., 2018; Sokolic et al., 2017; Matyasko and Chau, 2017) have attempted to use first-order approximation to estimate the input space margin. For first-order methods, the margin will be accurately estimated when the classification function is linear. MMA’s margin estimation is exact when the minimal length perturbation δ^* can be solved, which is not only satisfied by linear models, but also by a broader range of models, e.g. models that are convex w.r.t. input x . This relaxed condition could potentially enable more accurate margin

estimation which improves MMA training’s performance.

(Cross-)Lipschitz Regularization: Tsuzuku et al. (2018) enlarges their margin by controlling the global Lipschitz constant, which in return places a strong constraint on the model and harms its learning capabilities. Instead, our method, alike adversarial training, uses adversarial attacks to estimate the margin to the decision boundary. With a strong method, our estimate is much more precise in the neighborhood around the data point, while being much more flexible due to not relying on a global Lipschitz constraint.

Hard-Margin SVM (Vapnik, 2013) in the separable case: Assuming that all the training examples are correctly classified and using our notations on general classifiers, the hard-margin SVM objective can be written as:

$$\max_{\theta} \left\{ \min_i d_{\theta}(z_i) \right\} \quad \text{s.t.} \quad L_{\theta}(z_i) < 0, \forall i. \quad (7)$$

On the other hand, under the same “separable and correct” assumptions, MMA formulation in Eq. (5) can be written as

$$\max_{\theta} \left\{ \sum_i d_{\theta}(z_i) \right\} \quad \text{s.t.} \quad L_{\theta}(z_i) < 0, \forall i, \quad (8)$$

which is maximizing the *average* margin rather than the *minimum* margin in SVM. Note that the theorem on gradient calculation of the margin in Section 2.1 also applies to the SVM formulation of differentiable functions. Because of this, we can also use SGD to solve the following “SVM-style” formulation:

$$\max_{\theta} \left\{ \min_{i \in \mathcal{S}_{\theta}^+} d_{\theta}(z_i) - \sum_{j \in \mathcal{S}_{\theta}^-} J_{\theta}(z_j) \right\}. \quad (9)$$

As our focus is using MMA to improve adversarial robustness which involves maximizing the average margin, we delay the maximization of minimum margin to future work.

6 Conclusion

In this paper, we propose max-margin adversarial (MMA) training. We show that the input space margin can be maximized by minimizing the loss on the minimal length perturbation. This enables gradient descent on objectives that involve the input space margin. We propose a specific formulation of max-margin adversarial training to maximize the average margin motivated by improving adversarial robustness. Our experiments show that MMA trained models achieve state of the art adversarial robustness on the MNIST and CIFAR10 datasets under both ℓ_{∞} and ℓ_2 perturbations.

References

- Athalye, A., Carlini, N., and Wagner, D. (2018). Obfuscated gradients give a false sense of security: Circumventing defenses to adversarial examples. *arXiv preprint arXiv:1802.00420*.
- Biggio, B., Corona, I., Maiorca, D., Nelson, B., Šrndić, N., Laskov, P., Giacinto, G., and Roli, F. (2013). Evasion attacks against machine learning at test time. In *Joint European conference on machine learning and knowledge discovery in databases*, pages 387–402. Springer.

- Carlini, N. and Wagner, D. (2016). Defensive distillation is not robust to adversarial examples. *arXiv preprint arXiv:1607.04311*.
- Carlini, N. and Wagner, D. (2017a). Adversarial examples are not easily detected: Bypassing ten detection methods. *arXiv preprint arXiv:1705.07263*.
- Carlini, N. and Wagner, D. (2017b). Towards evaluating the robustness of neural networks. In *Security and Privacy (SP), 2017 IEEE Symposium on*, pages 39–57. IEEE.
- Cisse, M., Bojanowski, P., Grave, E., Dauphin, Y., and Usunier, N. (2017). Parseval networks: Improving robustness to adversarial examples. In *International Conference on Machine Learning*, pages 854–863.
- Elsayed, G. F., Krishnan, D., Mobahi, H., Regan, K., and Bengio, S. (2018). Large margin deep networks for classification. *arXiv preprint arXiv:1803.05598*.
- Hein, M. and Andriushchenko, M. (2017). Formal guarantees on the robustness of a classifier against adversarial manipulation. *arXiv preprint arXiv:1705.08475*.
- Huang, R., Xu, B., Schuurmans, D., and Szepesvári, C. (2015). Learning with a strong adversary. *arXiv preprint arXiv:1511.03034*.
- Madry, A., Makelov, A., Schmidt, L., Tsipras, D., and Vladu, A. (2017). Towards deep learning models resistant to adversarial attacks. *arXiv preprint arXiv:1706.06083*.
- Matyasko, A. and Chau, L.-P. (2017). Margin maximization for robust classification using deep learning. In *Neural Networks (IJCNN), 2017 International Joint Conference on*, pages 300–307. IEEE.
- Rony, J., Hafemann, L. G., Oliveira, L. S., Ayed, I. B., Sabourin, R., and Granger, E. (2018). Decoupling direction and norm for efficient gradient-based l2 adversarial attacks and defenses. *arXiv preprint arXiv:1811.09600*.
- Ross, A. S. and Doshi-Velez, F. (2017). Improving the adversarial robustness and interpretability of deep neural networks by regularizing their input gradients. *arXiv preprint arXiv:1711.09404*.
- Sokolic, J., Giryes, R., Sapiro, G., and Rodrigues, M. R. (2017). Robust large margin deep neural networks. *IEEE Transactions on Signal Processing*.
- Szegedy, C., Zaremba, W., Sutskever, I., Bruna, J., Erhan, D., Goodfellow, I., and Fergus, R. (2013). Intriguing properties of neural networks. *arXiv preprint arXiv:1312.6199*.
- Tsipras, D., Santurkar, S., Engstrom, L., Turner, A., and Madry, A. (2019). Robustness may be at odds with accuracy. In *International Conference on Learning Representations*.
- Tsuzuku, Y., Sato, I., and Sugiyama, M. (2018). Lipschitz-margin training: Scalable certification of perturbation invariance for deep neural networks. *arXiv preprint arXiv:1802.04034*.
- Vapnik, V. (2013). *The nature of statistical learning theory*. Springer science & business media.
- Yu, Y.-L. (2012). The differentiability of the upper envelop. *Technical note*.
- Zagoruyko, S. and Komodakis, N. (2016). Wide residual networks. *arXiv preprint arXiv:1605.07146*.

Appendix

A Proofs

A.1 Proof of theorem 2.1

Proof. Recall that $z = (x, y)$ and $\epsilon(\delta) = \|\delta\|$. Here we compute the gradient for $d_\theta(z)$ in its general form. Consider the following optimization problem:

$$d_\theta(z) = \min_{\delta \in \Delta(\theta)} \epsilon(\delta),$$

where $\Delta(\theta) = \{\delta : L_\theta(x + \delta, y) = 0\}$, ϵ and L_θ are both C^2 functions¹². Denotes its Lagrangian by $\mathcal{L}(\delta, \lambda)$, where

$$\mathcal{L}(\delta, \lambda) = \epsilon(\delta) + \lambda L_\theta(x + \delta, y)$$

For a fixed θ , the optimizer δ^* and λ^* must satisfy the first-order conditions (FOC)

$$\begin{aligned} \frac{\partial \epsilon(\delta)}{\partial \delta} + \lambda \frac{\partial L_\theta(x + \delta, y)}{\partial \delta} \Big|_{\delta=\delta^*, \lambda=\lambda^*} &= 0, \\ L_\theta(x + \delta, y) \Big|_{\delta=\delta^*} &= 0. \end{aligned} \tag{10}$$

Put the FOC equations in vector form,

$$G((\delta, \lambda), \theta) = \begin{pmatrix} \frac{\partial \epsilon(\delta)}{\partial \delta} + \lambda \frac{\partial L_\theta(x + \delta, y)}{\partial \delta} \\ L_\theta(x + \delta, y) \end{pmatrix} \Big|_{\delta=\delta^*, \lambda=\lambda^*} = 0.$$

Note that G is C^1 continuously differentiable since ϵ and L_θ are C^2 functions. Furthermore, the Jacobian matrix of G w.r.t (δ, λ) is

$$\begin{aligned} \nabla_{(\delta, \lambda)} G((\delta^*, \lambda^*), \theta) \\ = \begin{pmatrix} \frac{\partial^2 \epsilon(\delta^*)}{\partial \delta^2} + \lambda^* \frac{\partial^2 L_\theta(\delta^*)}{\partial \delta^2} & \frac{\partial L_\theta(\delta^*)}{\partial \delta} \\ \frac{\partial L_\theta(\delta^*)}{\partial \delta}^\top & 0 \end{pmatrix} \end{aligned}$$

which by assumption is full rank. Therefore, by the implicit function theorem, δ^* and λ^* can be expressed as a function of θ , denoted by $\delta^*(\theta)$ and $\lambda^*(\theta)$.

To further compute $\nabla_\theta d_\theta(z)$, note that $d_\theta(z) = \epsilon(\delta^*(\theta))$. Thus,

$$\nabla_\theta d_\theta(z) = \frac{\partial \epsilon(\delta^*)}{\partial \delta} \frac{\partial \delta^*(\theta)}{\partial \theta} = -\lambda^* \frac{\partial L_\theta(\delta^*)}{\partial \delta} \frac{\partial \delta^*(\theta)}{\partial \theta}, \tag{11}$$

where the second equality is by Eq. (10). The implicit function theorem also provides a way of computing $\frac{\partial \delta^*(\theta)}{\partial \theta}$ which is complicated involving taking inverse of the matrix $\nabla_{(\delta, \lambda)} G((\delta^*, \lambda^*), \theta)$. Here we present a relatively simple way to compute this gradient. Note that

$$L_\theta(\delta^*(\theta)) = 0.$$

¹²Note that a simple application of Danskin's theorem would not be valid as the constraint set $\Delta(\theta)$ depends on the parameter θ .

Differentiate with w.r.t. θ on both sides:

$$\frac{\partial L_\theta(\delta^*)}{\partial \theta} + \frac{\partial L_\theta(\delta^*)}{\partial \delta} \frac{\partial \delta^*(\theta)}{\partial \theta} = 0. \quad (12)$$

Combining Eq. (11) and Eq. (12),

$$\nabla_\theta d_\theta(z) = \lambda^*(\theta) \frac{\partial L_\theta(\delta^*)}{\partial \theta}. \quad (13)$$

Lastly, note that

$$\left\| \frac{\partial \epsilon(\delta)}{\partial \delta} + \lambda \frac{\partial L_\theta(x + \delta, y)}{\partial \delta} \Big|_{\delta=\delta^*, \lambda=\lambda^*} \right\|_2 = 0.$$

Therefore, one way to calculate $\lambda^*(\theta)$ is by

$$\lambda^*(\theta) = \frac{\frac{\partial \epsilon(\delta)}{\partial \delta}^\top \frac{\partial L_\theta(x + \delta, y)}{\partial \delta}}{\frac{\partial L_\theta(x + \delta, y)}{\partial \delta}^\top \frac{\partial L_\theta(x + \delta, y)}{\partial \delta}} \Big|_{\delta=\delta^*}$$

□

A.2 A lemma for later proofs

The following lemma helps relate the objective of adversarial training with that of our MMA training. Here, we denote $L_\theta(x + \delta, y)$ as $L_\theta(\delta)$ for simplicity.

Lemma A.1. *Given (x, y) and θ , assume that $L_\theta(\delta)$ is continuous in δ , then for $\epsilon \geq 0$, and $\ell \geq L_\theta(0) \in \text{Range}(L_\theta)$, it holds that*

$$\min_{L_\theta(\delta) \geq \ell} \|\delta\| = \epsilon \implies \max_{\|\delta\| \leq \epsilon} L_\theta(\delta) = \ell; \quad (14)$$

$$\max_{\|\delta\| \leq \epsilon} L_\theta(\delta) = \ell \implies \min_{L_\theta(\delta) \geq \ell} \|\delta\| \leq \epsilon. \quad (15)$$

Proof. Eq. (14). We prove this by contradiction. Suppose $\max_{\|\delta\| \leq \epsilon} L_\theta(\delta) > \ell$. When $\epsilon = 0$, this violates our assumption $\ell \geq L_\theta(0)$ in the theorem. So assume $\epsilon > 0$. Since $L_\theta(\delta)$ is a continuous function defined on a compact set, the maximum is attained by $\bar{\delta}$ such that $\|\bar{\delta}\| \leq \epsilon$ and $L_\theta(\bar{\delta}) > \ell$. Note that L_θ is continuous and $\ell \geq L_\theta(0)$, then there exists $\tilde{\delta} \in \langle 0, \bar{\delta} \rangle$ i.e. the line segment connecting 0 and $\bar{\delta}$, such that $\|\tilde{\delta}\| < \epsilon$ and $L_\theta(\tilde{\delta}) = \ell$. This follows from the intermediate value theorem by restricting $L_\theta(\delta)$ onto $\langle 0, \bar{\delta} \rangle$. This contradicts $\min_{L_\theta(\delta) \geq \ell} \|\delta\| = \epsilon$.

If $\max_{\|\delta\| \leq \epsilon} L_\theta(\delta) < \ell$, then $\{\delta : \|\delta\| \leq \epsilon\} \subset \{\delta : L_\theta(\delta) < \ell\}$. Every point $p \in \{\delta : \|\delta\| \leq \epsilon\}$ is in the open set $\{\delta : L_\theta(\delta) < \ell\}$, there exists an open ball with some radius r_p centered at p such that $B_{r_p} \subset \{\delta : L_\theta(\delta) < \ell\}$. This forms an open cover for $\{\delta : \|\delta\| \leq \epsilon\}$. Since $\{\delta : \|\delta\| \leq \epsilon\}$ is compact, there is an open finite subcover \mathcal{U}_ϵ such that: $\{\delta : \|\delta\| \leq \epsilon\} \subset \mathcal{U}_\epsilon \subset \{\delta : L_\theta(\delta) < \ell\}$. Since \mathcal{U}_ϵ is finite, there exists $h > 0$ such that $\{\delta : \|\delta\| \leq \epsilon + h\} \subset \{\delta : L_\theta(\delta) < \ell\}$. Thus $\{\delta : L_\theta(\delta) \geq \ell\} \subset \{\delta : \|\delta\| > \epsilon + h\}$, contradicting $\min_{L_\theta(\delta) \geq \ell} \|\delta\| = \epsilon$ again.

Eq. (15). Assume that $\min_{L_\theta(\delta) \geq \ell} \|\delta\| > \epsilon$, then $\{\delta : L_\theta(\delta) \geq \ell\} \subset \{\delta : \|\delta\| > \epsilon\}$. Taking complementary set of both sides, $\{\delta : \|\delta\| \leq \epsilon\} \subset \{\delta : L_\theta(\delta) < \ell\}$. Therefore, by the compactness of $\{\delta : \|\delta\| \leq \epsilon\}$, $\max_{\|\delta\| \leq \epsilon} L_\theta(\delta) < \ell$, contradiction. □

A.3 Proof of theorem 2.2

Proof. By the definition of θ_{adv} ,

$$\max_{\|\delta\| \leq \epsilon^*} L_{\theta_{\text{MMA}}}(\delta) \geq \max_{\|\delta\| \leq \epsilon^*} L_{\theta_{\text{adv}}}(\delta).$$

We further prove it is not possible that

$$\max_{\|\delta\| \leq \epsilon^*} L_{\theta_{\text{MMA}}}(\delta) > \max_{\|\delta\| \leq \epsilon^*} L_{\theta_{\text{adv}}}(\delta).$$

If so, by the first implication in Lemma A.1 and the definition of ϵ^* , we have

$$\ell = \max_{\|\delta\| \leq \epsilon^*} L_{\theta_{\text{MMA}}}(\delta) > \max_{\|\delta\| \leq \epsilon^*} L_{\theta_{\text{adv}}}(\delta),$$

and thus with similar arguments to the proof of Lemma A.1,

$$\min_{L_{\theta_{\text{adv}}}(\delta) \geq \ell} \|\delta\| > \epsilon^* = \|\delta^*(\theta_{\text{MMA}})\|,$$

contradicting the definition of θ_{MMA} . Therefore,

$$\max_{\|\delta\| \leq \epsilon^*} L_{\theta_{\text{MMA}}}(\delta) = \max_{\|\delta\| \leq \epsilon^*} L_{\theta_{\text{adv}}}(\delta).$$

□

A.4 Proof of Theorem 2.3

Proof. By the definition of θ_{MMA} ,

$$\min_{L_{\theta_{\text{MMA}}}(\delta) \geq \ell^*} \|\delta\| \geq \min_{L_{\theta_{\text{adv}}}(\delta) \geq \ell^*} \|\delta\|.$$

We further prove it is not possible that

$$\min_{L_{\theta_{\text{MMA}}}(\delta) \geq \ell^*} \|\delta\| > \min_{L_{\theta_{\text{adv}}}(\delta) \geq \ell^*} \|\delta\|.$$

If so, by the no overshooting assumption,

$$\min_{L_{\theta_{\text{MMA}}}(\delta) \geq \ell^*} \|\delta\| > \epsilon.$$

and thus with similar arguments to the proof of the second implication in Lemma A.1,

$$\max_{\|\delta\| \leq \epsilon} L_{\theta_{\text{MMA}}}(\delta) < \ell^*,$$

contradicting the definition of θ_{adv} . Therefore,

$$\max_{\|\delta\| \leq \epsilon^*} L_{\theta_{\text{MMA}}}(\delta) = \max_{\|\delta\| \leq \epsilon^*} L_{\theta_{\text{adv}}}(\delta).$$

□

A.5 Proof of Proposition 2.1

Since θ_0 is not a local minimum, there exists a direction d , such that $L'(\delta^*, \theta_0; \vec{d}) = \frac{\partial L(\delta^*, \theta_0 + t\vec{d})}{\partial t}$ is negative. The next theorem provides a way to compute the directional gradient along this direction d .

Theorem A.1 (Danskin). *Fix a direction $\vec{d} \in \Theta$, $\epsilon > 0$, $t \in [0, 1]$ and $\theta_0 \in \Theta$. Let $\ell_{\theta_0, \vec{d}, \epsilon}(t) := \sup_{\delta \in [-\epsilon, \epsilon]^d} L(\delta, \theta_0 + t\vec{d})$. Then the derivative of $\ell_{\vec{d}, \epsilon, \theta_0}(t)$ exists and is given by:*

$$\ell'_{\vec{d}, \epsilon, \theta_0}(t) = L'(\delta^*, \theta_0; \vec{d}).$$

Proof. [Proof sketch] We basically apply a version of Danskin theorem for directional absolutely continuous maps and semi-continuous maps (Yu, 2012). 1. the constraint set is $[-\epsilon, \epsilon]^d$ is compact; 2. $L(\theta_0 + t\vec{d}; x + \delta, y)$ is piecewise Lipschitz and hence absolutely continuous (an induction argument on the integral representation over the finite pieces). 3. $L(\theta_0 + t\vec{d}; x + \delta, y)$ is continuous on both δ and along the direction \vec{d} and hence upper semi continuous. Hence we can apply Theorem 1 in Yu (2012). \square

A.6 Proof of Proposition 2.2

Since f_{θ_0} has a margin ϵ_0 , thus

$$\max_{\delta \in [-\epsilon_0, \epsilon_0]^d} L(\theta_0; x + \delta, y) = 0$$

Further by $\ell_{\theta_0, \vec{d}, \epsilon_0}(t) \leq \ell_{\theta_0, \vec{d}, \epsilon_0}(0)$,

$$\sup_{\delta \in [-\epsilon, \epsilon]^d} L(\delta, \theta_0 + t\vec{d}) \leq \sup_{\delta \in [-\epsilon, \epsilon]^d} L(\delta, \theta_0).$$

To see the equality (constraint not binding), we use the following argument. The envelope function's continuity is passed from the continuity of $L(\theta_0; x + \delta, y)$. The inverse image of a closed set under continuous function is closed. If δ^* lies in the interior of $\max_{\delta \in [-\epsilon_0, \epsilon_0]^d} L_{\vec{d}, \epsilon}(\theta_0; x + \delta, y) \geq 0$, we would have a contradiction. Therefore the constraint is not binding, due to the continuity of the envelope function. By Eq. (4), $\max_{\delta \in [-\epsilon_0, \epsilon_0]^d} L(\theta_1; x + \delta, y) < 0$. So for the parameter θ_1 , f_{θ_1} has a margin $\epsilon_1 > \epsilon_0$.

B Detailed Settings for Training

The LeNet5 is composed of 32-channel conv filter + ReLU + size 2 max pooling + 64-channel conv filter + ReLU + size 2 max pooling + fc layer with 1024 units + ReLU + fc layer with 10 output classes. We do not preprocess MNIST images before feeding into the model.

For training LeNet5 on all MNIST experiments, for both PGD and MMA training, we use the Adam optimizer with an initial learning rate of 0.0001 and train for 100000 steps with batch size 50. In our initial experiments, we tested different initial learning rate at 0.0001, 0.001, 0.01, and 0.1 and do not find noticeable differences.

We use the WideResNet-28-4 as described in [Zagoruyko and Komodakis \(2016\)](#) for our experiments, where 28 is the depth and 4 is the widen factor. We use “per image standardization”¹³ to preprocess CIFAR10 images, following [Madry et al. \(2017\)](#).

For training WideResNet on CIFAR10 variants, we use stochastic gradient descent with momentum 0.9 and weight decay 0.0002. We train 50000 steps in total with batch size 128. The learning rate is set to 0.3 at step 0, 0.09 at step 20000, 0.03 at step 30000, and 0.009 at step 40000. This setting is the same for PGD and MMA training. In our initial experiments, we tested different learning rate at 0.03, 0.1, 0.3, and 0.6, and kept using 0.3 for all our later experiments. We also tested a longer training schedule, following [Madry et al. \(2017\)](#), where we train 80000 steps with different learning rate schedules. We did not observe improvement with this longer training, therefore kept using the 50000 steps training.

For models trained on MNIST, we use 40-step PGD attack with the soft logit margin (SLM) loss defined in Section 3, for CIFAR10 we use 10 step PGD, also with the SLM loss. In AN-PGD, we always perform 10 step binary search after PGD, with the SLM loss. For AN-PGD, the maximum perturbation length is always 1.05 times the hinge threshold: $\epsilon_{max} = 1.05d_{max}$. The initial perturbation length at the first epoch, ϵ_{init} , have different values under different settings. $\epsilon_{init} = 0.5$ for MNIST ℓ_2 , $\epsilon_{init} = 0.1$ for MNIST ℓ_∞ , $\epsilon_{init} = 0.5$ for CIFAR10 ℓ_2 , $\epsilon_{init} = 0.05$ for CIFAR10 ℓ_2 . In epochs after the first, ϵ_{init} will be set to the margin of the same example from last epoch.

C Detailed Comparison with Adversarial Training with DDN

Here we make more detailed comparison between our work and the concurrent DDN attack / training described in [Rony et al. \(2018\)](#).

The DDN MNIST model is a larger ConvNet with similar structure to our LeNet5, and the CIFAR10 model is wideresnet-28-10, which is similar but larger than the wideresnet-28-4 that we use.

DDN training is very similar to MMA training with a few differences. DDN training is “training on adversarial examples generated by the DDN attack”. When DDN attack does not find a successful adversarial example, it returns the clean image, and the model will use it for training. In MMA, when a successful adversarial example cannot be found, it is treated as a perturbation with very large magnitude, we will be ignored by the hinge loss when we calculate gradient for this example. Also in DDN training, there exist a maximum norm of the perturbation. This maximum norm constraint does not exist for MMA training. When a perturbation is larger than the hinge threshold, it will be ignored by the hinge loss. There are also a few differences in training hyperparameters, which we refer the reader to [Rony et al. \(2018\)](#) for details.

Despite these differences, in our experiments MMA training achieves similar performances under the ℓ_2 cases. While DDN attack and training only focus on ℓ_2 cases, we also show that the MMA training framework provides significant improvements over PGD training.

¹³Description can be found at https://www.tensorflow.org/api_docs/python/tf/image/per_image_standardization. We implemented our own version in PyTorch.

Table 3: Accuracy and Robustness of models under ℓ_∞ training. In the model column, STD stands for standardly trained model. M- d_{\max} represents the MMA trained model with hinge threshold d_{\max} . PL- ϵ represents the PGD trained model with linear magnitude scaling. P- ϵ represents the PGD trained model with fixed ϵ magnitude. PGDm shows the performances reported in [Madry et al. \(2017\)](#). CE represents robust accuracies after 50 random starts of PGD attacks cross-entropy loss. CW represents robust accuracies after 50 random starts of PGD attacks with CW loss. BOTH represents the accuracy under combined CE and CW (100 random starts) PGD attacks.

MNIST MODEL	Acc	Acc AT $\epsilon = 0.3$			Acc AT $\epsilon = 0.4$		
		CE	CW	BOTH	CE	CW	BOTH
STD	99.2	0.0	0.0	0.0	0.0	0.0	0.0
M-0.45	99.0	93.7	93.7	93.6	89.0	89.1	88.6
PL-0.45	98.9	94.3	94.4	94.2	90.2	90.3	89.9
PL-0.4	99.0	93.8	93.9	93.8	89.5	89.7	89.2
PL-0.35	99.0	92.7	92.8	92.7	31.2	32.4	30.0
PL-0.3	99.1	90.5	90.6	90.4	0.9	0.9	0.7
P-0.4	96.6	88.7	88.7	88.5	84.6	84.5	84.1
P-0.35	99.0	93.2	93.2	93.2	33.8	37.3	32.5
P-0.3	99.0	91.7	91.7	91.6	1.8	2.1	1.6
PGDm ¹⁴	98.8	89.6	89.7	–	–	–	–
CIFAR MODEL	Acc	Acc AT $\epsilon = 8/255$			Acc AT $\epsilon = 16/255$		
		CE	CW	BOTH	CE	CW	BOTH
STD	94.9	0.0	0.0	0.0	0.0	0.0	0.0
M-32	85.8	55.2	54.9	54.0	41.5	38.9	37.8
M-20	87.0	53.3	53.6	52.3	35.9	33.5	32.4
M-16	87.7	52.3	52.9	51.1	33.7	32.8	30.6
M-12	88.7	49.2	49.8	48.4	26.2	24.7	23.6
M-8	89.8	43.7	43.6	42.5	16.2	13.9	13.0
PL-20	65.8	48.3	45.1	44.8	30.5	26.4	25.3
PL-16	70.7	51.0	48.2	47.7	28.5	26.1	24.8
PL-12	79.4	51.8	50.2	49.2	23.5	23.1	21.3
PL-8	85.6	49.8	49.1	47.7	16.6	17.3	15.6
P-20	61.1	46.3	43.4	43.2	31.8	27.6	26.7
P-16	77.9	51.8	49.9	49.0	24.5	24.0	22.1
P-12	68.9	50.0	47.2	46.7	29.5	26.8	25.4
P-8	85.1	50.0	49.2	47.9	16.9	17.5	15.7
PGDm ¹⁵	87.3	45.2	–	–	–	–	–

D Full Tables

Here we provide the full version of the tables in Table 3 and Table 4.

¹⁴Model from [Madry et al. \(2017\)](#). The accuracies of “100-step PGD on the cross-entropy loss with 50 random restarts” is from github.com/MadryLab/mnist_challenge/

¹⁵Model from [Madry et al. \(2017\)](#). The accuracy of “20-step PGD on the cross-entropy loss with 10 random restarts” is from github.com/MadryLab/cifar10_challenge/

Table 4: Accuracy and Robustness of models under ℓ_2 training. In the model column, STD, M- d_{\max} , PL- ϵ , P- ϵ have the same meaning as those in Table 3. DNN represents our evaluation on models from Rony et al. (2018) ASR is attack success rate (lower the better). DDN represents the ASR/mean norm after DDN attack with 1000 iterations. CW represents the ASR/mean norm after CW attack 9×10000 iterations. BOTH represents the ASR/mean norm after picking the stronger attack among DDN and CW attack.

MNIST MODEL	Acc	ASR			MEAN ℓ_2		
		DDN	CW	BOTH	DDN	CW	BOTH
STD	99.2	100.0	100.0	100.0	1.62	1.65	1.61
M-8	98.2	100.0	99.8	100.0	2.72	2.81	2.71
M-6	98.3	100.0	99.0	100.0	2.72	2.85	2.71
M-4	98.5	100.0	98.6	100.0	2.68	2.80	2.67
M-2	99.3	100.0	100.0	100.0	2.24	2.26	2.23
PL-4	93.7	100.0	100.0	100.0	2.82	2.67	2.57
PL-3	97.5	100.0	100.0	100.0	2.64	2.66	2.56
PL-2	99.4	100.0	100.0	100.0	1.96	1.95	1.94
PL-1	99.1	100.0	100.0	100.0	2.30	2.32	2.28
P-4	93.4	100.0	100.0	100.0	2.84	2.68	2.57
P-3	97.1	100.0	100.0	100.0	2.67	2.69	2.58
P-2	98.8	100.0	100.0	100.0	2.39	2.43	2.37
P-1	99.3	100.0	100.0	100.0	2.04	2.04	2.02
DDN	99.0	100.0	100.0	100.0	2.61	2.63	2.57
CIFAR MODEL	Acc	ASR			MEAN ℓ_2		
		DDN	CW	BOTH	DDN	CW	BOTH
STD	94.9	100.0	100.0	100.0	0.10	0.09	0.09
M-7	78.0	96.2	100.0	100.0	1.67	1.14	0.99
M-5	80.6	97.0	100.0	100.0	1.77	1.13	0.97
M-3	83.8	98.4	100.0	100.0	1.13	1.11	1.00
M-2	85.5	99.8	100.0	100.0	0.96	1.01	0.95
M-1	89.4	100.0	100.0	100.0	0.82	0.84	0.82
PL-3	61.5	100.0	100.0	100.0	1.30	1.16	1.13
PL-2	72.1	100.0	100.0	100.0	1.22	1.17	1.13
PL-1	83.6	100.0	100.0	100.0	1.01	1.02	0.97
P-3	59.1	100.0	100.0	100.0	1.29	1.14	1.11
P-2	71.1	100.0	100.0	100.0	1.21	1.17	1.12
P-1	83.2	100.0	100.0	100.0	1.01	1.03	0.98
DDN	89.1	100.0	100.0	100.0	0.86	0.89	0.86